phys. stat. sol. (c) **5**, No. 9, 2704–2708 (2008) / **DOI** 10.1002/pssc.200779293

physica status solidi c
www.pss-c.com
current topics in solid state physics

Fabrication of radial superlattices based on different hybrid materials

Christoph Deneke[*, 1], Joachim Schumann[1], Ronny Engelhard[1], Jürgen Thomas[2], Wilfried Sigle[3], Ute Zschieschang[4], Hagen Klauk[4], Andrey Chuvilin[5], and Oliver G. Schmidt[1]

[1] Institute for Integrative Nanosciences, IFW Dresden, Helmholtzstr. 20, 01169 Dresden, Germany
[2] Institute for Complex Materials, IFW Dresden, Helmholtzstr. 20, 01169 Dresden, Germany
[3] Max-Planck-Institut für Metallforschung, Heisenbergstr. 3, 70569 Stuttgart, Germany
[4] Max-Planck-Institut für Festkörperforschung, Heisenbergstr. 1, 70569 Stuttgart, Germany
[5] Universität Ulm, Albert-Einstein-Allee 11, 89081 Ulm, Germany

Received 23 October 2007, revised 21 December 2007, accepted 28 December 2007
Published online 13 June 2008

PACS 68.65.Cd, 81.07.–b

[*] Corresponding author: e-mail c.deneke@ifw-dresden.de, Phone: +49 351 4659 751, Fax: +49 351 4659 782

The fabrication of radial superlattices is demonstrated for three different hybrid material systems. Inherently strained pseudomorphic InGaAs/Fe_3Si bilayers are rolled-up to produce radial semiconductor/magnetic heterostructures. Apart from this epitaxially based material system, radial InAlGaAs/GaAs/Cr superlattices are investigated as an example for periodic semiconductor/metallic multilayers. Finally, rolled-up InGaAs/GaAs/1-hexadecanethiol layers are studied as a new class of semiconductor/organic short-period superlattices. The radial superlattices are examined structurally, and particular attention is paid to the interfaces of the periodic hybrid heterostructures. These investigations reveal that, except for the semiconductor/organic hybrid material system, always a new interface layer forms, modifying the initial rolled-up layer system. The study demonstrates the potential to fabricate periodic layer systems from pure single-crystalline material, single-crystalline/poly-crystalline material as well as single-crystalline/non-crystalline material, which cannot be realized by any planar growth techniques.

1 Introduction The invention and realization of planar superlattices have attracted overwhelming interest for both fundamental as well as application-related research over more than 30 years [1]. The great success of this technology relies on the ability to repetitively grow ultrathin multilayers and heterostructures with a precision of a single monolayer. Such superlattices give rise to quantum size effects modifying their fundamental optical, electronic or magnetic properties [1], and have become the backbone of a whole new generation of heterojunction based devices. More recently, a new class of integrative hybrid radial superlattices [2-5] has been realized by the roll-up of strained layer systems on a chip [6, 7]. These radial superlattices have been realized out of various hybrid material combinations such as semiconductor/organic [3], Si/SiO_x [4], or semiconductor/metal [5] layer systems. The term radial superlattice is used in the sense that − similar to a planar superlattice − an initial layer system is periodically repeated in one spatial (here: radial) direction. The periods of the formed multilayer stack are thin enough to allow for electronic, magnetic, or electromagnetic coherence across the radial superlattice. Due to the combination of the radial symmetry [8] and the periodic modulation of the physical properties, new functionalities in electronic, optoelectronic, X-ray, fluidic, magnetoelectronic active as well as passive devices are imaginable.

In this paper, the fabrication of radial superlattices by rolled-up nanotech is demonstrated for three different hybrid material combinations. A pseudomorphic InGaAs/Fe_3Si layer system is used to fabricate a radial superlattice out of strained epitaxial bilayers [2]. To demonstrate the generality of rolled-up nanotech, we extend this technology to non-epitaxial layer systems such as InGaAs/GaAs/Cr and InGaAs/GaAs/1-hexadecanethiol. For all material systems, only the initial period is fabricated by the combination of different deposition techniques. The

short-period superlattice is then formed by the roll-up process. This process is fundamentally different compared to techniques where the initial layer sequence is repeated by the same growth technique several times. The rolled-up radial structures are studied in detail by various electron microscopy techniques in combination with chemical analysis. Special attention is paid to the interfaces of the periodic multilayers. Except for the rolled-up InGaAs/GaAs/1-hexadecanethiol, the formation of new interface layers is observed for all other layer systems. In the case of the radial InGaAs/GaAs/Cr superlattice, detailed electron energy-loss spectroscopy demonstrates that the interface formation is mainly due to oxidation of the Cr layer. In the case of the radial InGaAs/Fe_3Si superlattice, interface formation is mainly caused by imperfect bonding between neighbouring windings.

2 Experimental All strained layer systems are fabricated by the combination of III-V molecular beam epitaxy (MBE) with other deposition methods on GaAs (001) substrates. The MBE layers typically consist of a 10–20 nm thick AlAs sacrificial layer, followed by a 20 nm $In_{0.2}Ga_{0.8}As$, a 3 nm $In_{0.2}Al_{0.2}Ga_{0.6}As$/ 3 nm GaAs or a 2 nm $In_{0.33}Ga_{0.67}As$/ 4.5 nm GaAs layer. After MBE growth the samples are removed from the ultra-high-vacuum (UHV) chamber and additional layers are deposited on top of the III-V heterostructures. To form an expitaxial layer system, the III-V surface is thermally deoxidized and a 20 nm Fe_3Si is grown pseudomorphically on top of the InGaAs layer. To create a semiconductor/metal initial layer system, 7 nm Cr are deposited by thermal evaporation onto the untreated strained InAlGaAs/GaAs bilayer. Fabrication of a semiconductor/organic hybrid trilayer is achieved by the self-assembly of a 1-hexadecanethiol monolayer on top of the InGaAs/GaAs bilayer [10].

Tube formation is initiated by selective wet chemical removal of the sacrificial AlAs layer with diluted HF. To investigate the rolled-up micro- and nanotubes, tube cross-sections are carefully prepared by focused ion beam (FIB) etching using a Zeiss nVision or a FEI Strata dual beam machine, respectively [9]. Both FIB machines offer the possibility to acquire scanning electron microscopy (SEM) images of the rolled-up structure.

For the InGaAs/Fe_3Si radial superlattice high-angle annular dark field (HAADF) scanning electron transmission microscopy (STEM), selected-area electron diffraction (SAED) and energy-filtered transmission electron microscopy (EFTEM) were carried out in a FEI Tecnai F30 equipped with a Gatan GIF at an acceleration voltage of 300 kV. Bright field (BF) STEM as well as electron energy-loss spectroscopy (EELS) was performed for the InAlGaAs/GaAs/Cr superlattice in a VG HB501 UX dedicated STEM equipped a with Gatan ENFINA EELS spectrometer at an acceleration voltage of 100 kV (probe size below 1 nm). The high-resolution transmission electron microscopy (HRTEM) images of the InGaAs/GaAs/thiol superlattice were acquired by a FEI Titan 80-300 with an acceleration voltage of 300 kV.

3 Results and discussion Figure 1(a) shows a SEM image of a rolled-up InGaAs/Fe_3Si bilayer. The bilayer has performed multiple rotations on the substrate surface forming a tightly wound up tube with a diameter of 2 μm. The combination of III-V heterostructures with Fe_3Si has attracted some attention in recent years to realize spin injection into semiconductors [11, 12]. Figure 1(a) demonstrates that it is possible to integrate the magnetic material into a three-dimensional micro- and nano-architecture based on the deterministic release and rearrangement of thin solid films [13, 14], potentially providing additional functionality.

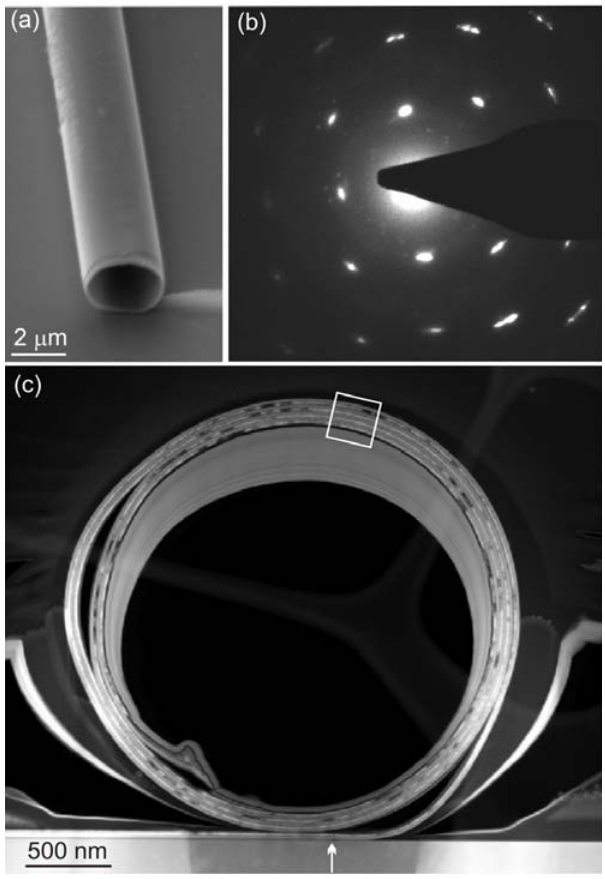

Figure 1 (a) SEM image of a rolled-up InGaAs/Fe_3Si bilayer. The rolled-up tube has a diameter of 2 μm. (b) SAED pattern obtained at the cross-section position of the rolled-up InGaAs/Fe_3Si tube marked in (c). The pattern clearly shows that the tube consists of a single-crystalline epitaxial material. (c) HAADF-STEM image of the rolled-up InGaAs/Fe_3Si tube prepared by FIB. The rolled-up tube with four separated windings is clearly visible. At two positions the windings are not tightly joined together.

In Fig. 1(c), an HAADF-STEM image of a cross-section of a rolled-up InGaAs/Fe_3Si tube embedded in the material deposited during FIB preparation is shown. The

STEM image allows for clear identification of the InGaAs/Fe_3Si bilayer, which has performed 4 windings during roll-up. The bilayer is still attached to unetched regions of the sample (marked by the white arrow). This demonstrates that the lateral position of the rolled-up layer system can be determined by the etching time [15]. At two positions, the detached bilayer did not bond back to itself leaving two voids in the tube wall. At all other positions, the rolled-up InGaAs/Fe_3Si bilayer is tightly joined together and forms a radial superlattice out of the semiconductor/magnetic hybrid material [11]. In principle, the observed voids in the radial superlattice should not hinder any technical applications of the structure. For phenomena relying on interaction effects between neighbouring windings, the voids should only lower the magnitude of the effect. For applications relying on the radial geometry, such voids have to be avoided by careful optimization of the roll-up process to obtain tightly wound structures. The InGaAs layer shows no contrast modulation over the whole rolled-up area, whereas in the Fe_3Si layer some darker regions are observed.

Figure 1(b) shows the SAED diffraction pattern obtained at the marked position (white rectangle in Fig. 1(c)) of the rolled-up layer stack. The pattern confirms that the crystalline pseudomorphic structure of the initial layer system stays undamaged during roll-up, and the rolled-up tube inherits the crystal structure of the epitaxial layers. The diffraction reflections are slightly elongated due to the curvature of the crystal layers, revealing the new radial symmetry of the rolled-up layers [5, 8].

To further investigate the chemical composition and the interface quality as well as to clarify the origin of the contrast modulation of the Fe_3Si layer of the radial InGaAs/Fe_3Si superlattice, an EFTEM study in the marked area of Fig. 1(c) was carried out.

Figure 2(a) presents the zero loss EFTEM image of the InGaAs/Fe_3Si layer stack. The top-most layer appears homogeneous without any major contrast modulation (bright layer) whereas the second layer of the layer stack (darker layer) shows pronounced contrast modulation in the Fe_3Si material indicating a defect. The thickness of both layers is measured as 20 nm showing that the InGaAs as well as the Fe_3Si layers are practically not thinned by the wet chemical etching process. Furthermore, the interface between neighboring periods of the superlattice can be identified. Such interfaces have also been observed in radial InGaAs/GaAs superlattices and are attributed to interfacial oxide formation [2, 8, 16] or imperfect bonding between two windings of the radial superlattice [3]. The single-crystallinity of the epitaxial initial layer system is signified by the minimum contrast modulation of both layers in the defect-free areas. The EFTEM image in Fig. 2(b) represents the iron distribution in the radial superlattice confirming that the dark layer in Fig. 2(a) is the Fe_3Si layer and the bright layer in Fig. 2(a) is the InGaAs layer. The iron contribution is homogeneous over the whole Fe_3Si layer indicating that the observed growth defect in Fig. 2(a) stems from an iron rich phase. To better identify interfaces in the radial superlattice, an EFTEM image at a low energy-loss (58 eV) was obtained (Fig. 2(c)). Besides the interfaces between succeeding periods of the superlattice, the growth interface between the InGaAs and Fe_3Si layer is hardly visible. Figure 2(d) presents an EFTEM image of the oxygen distribution in the radial superlattice. Large amounts of oxygen are found only at the outside of the superlattice and at the defect area of the Fe_3Si layer. Only a very weak oxygen signal is observed at the interfaces between neighbouring windings.

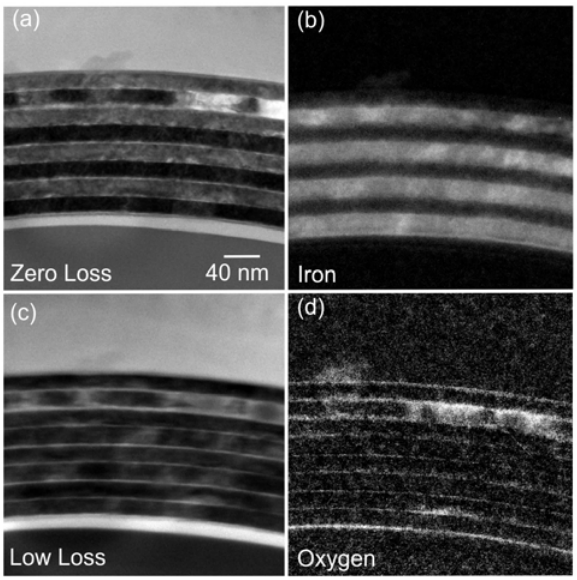

Figure 2 (a) Zero-loss EFTEM image of the area marked in Fig. 1. Two layers can be clearly identified by their different weight contrast, forming the radial superlattice. (b) EFTEM image at the iron L-edge at the same position allowing for identification of the InGaAs (dark) and the Fe_3Si layer (bright). (c) EFTEM image for a low energy-loss (58 eV) at the same position. The image allows for a clear identification of the different interfaces between the InGaAs and the Fe_3Si layers. (d) EFTEM image taken at the oxygen K-edge at the same position. Only a weak oxygen signal is detected at the interfaces. A strong oxygen signal is present at the defect position in the Fe_3Si layer seen in (a).

From this EFTEM study we conclude that the bonding interface at two succeeding periods of the radial InGaAs/Fe_3Si superlattice is mainly caused by the crystal misalignment. This is in contrast to rolled-up InGaAs/GaAs heterostructures where interfaces are more significantly generated by oxide formation [2, 8, 16]. The observed defects in the HAADF-STEM image (Fig. 1(c)) and the EFTEM images (Fig. 2(a) and 2(d)) are attributed to iron oxide formation during growth of the Fe_3Si layer. Since HRTEM images (not shown here) and SAED (Fig. 1(b)) indicate a pseudomorphic Fe_3Si layer on top of the InGaAs template, we attribute the defect formation and the visible InGaAs/Fe_3Si interface in Fig. 2(c) to an incomplete oxide removal and an InGaAs surface roughening during thermal deoxidation prior to the Fe_3Si growth. It is well known [11,

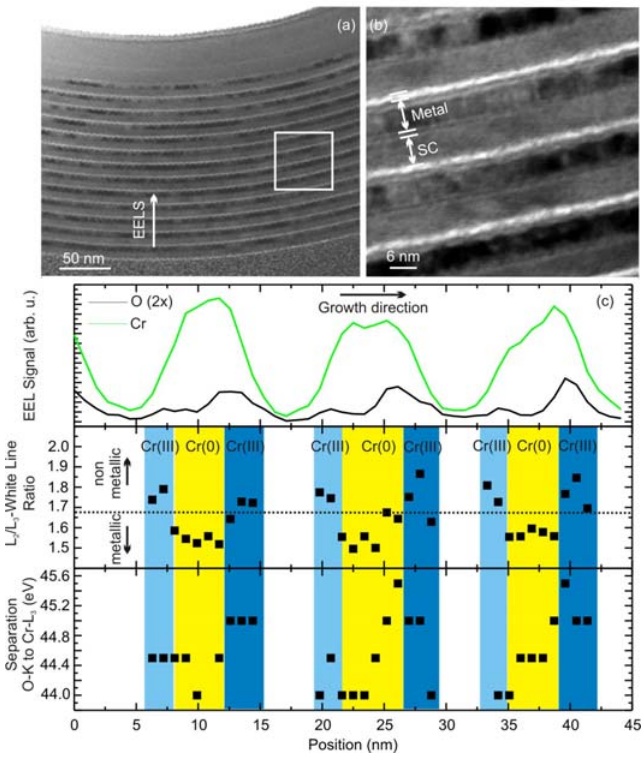

Figure 3 (a) BF-STEM image of a radial InAlGaAs/GaAs/Cr superlattice with 13 periods. The direction of a detailed EELS linescan as well as the area of a magnified image (3(b)) are indicated. (b) Magnified BF-STEM image of several periods of the radial InAlGaAs/GaAs/Cr superlattice. The different materials as well as two interface regions can be identified. (c) Integrated EEL signal of oxygen and chromium over three periods of the radial superlattice. Besides the integrated EEL signal, the ratio of the Cr-L_2- and Cr-L_3-white lines is determined in addition to the shift of the Cr-L_3-white line relative to the O-K-edge.

12] that Fe_3Si can be grown with high quality on top of a III-V template and therefore these imperfections can be overcome by a more optimized growth conditions.

Figures 3(a) and 3(b) present BF-STEM images obtained from a FIB-prepared cross-section of a rolled-up InAlGaAs/GaAs/Cr layer system. 13 periods of the radial InAlGaAs/GaAs/Cr superlattice can be identified due to the different material contrast of the semiconductor layer and the metal in Fig. 3(a). Again, the superlattice is embedded into material deposited during FIB preparation. The semiconductor layer shows no contrast modulation as expected for a single-crystalline material whereas the metal layer shows the typical contrast modulation of a polycrystalline material. The total layer stack has a thickness of 170 nm. This is in good agreement with the expected thickness from the initially grown layer system performing 13 rotations during roll-up. Besides the initial layers, at least one newly formed interface layer can already be observed in this semiconductor/metal hybrid radial superlattice.

Detailed investigation by BF-STEM (Fig. 3(b)) allows for the exact localization of any interfaces in the radial superlattice. A first, thicker interface between neighbouring windings is found between the Cr (marked as metal layer) and the InAlGaAs/GaAs bilayers (marked with SC). Additionally, a second, thinner interface layer between the single-crystalline InAlGaAs/GaAs bilayer and the polycrystalline Cr layer within the initial grown layer system can be identified. The thicknesses of the interfaces are determined as 1.3 nm and 0.8 nm, respectively. These values are in good agreement with previous HRTEM studies (see Ref. [5]).

To clarify the nature of the two newly formed interface layers, EELS was carried out over 3 periods of the radial superlattice. Figure 3(c) displays the results of this EEL analysis. Along with the integrated chromium signal, the integrated oxygen signal is monitored. From the EELS data the Cr-L_2- and Cr-L_3-white lines as well as the O-K-edge are deduced and the ratio between the Cr-L_2- and Cr-L_3-white lines is determined. Together with the separation of the Cr-L_3-edge from the O-K-edge, the data is used to approximate the valence state of the Cr [17] and is indicated in Fig. 3(c). The analysis shows that the central part of the Cr layer is metallic as expected from the deduced element profile. For the outer parts, the analysis reveals a higher Cr valence state typical for chromium oxide. The rise in the Cr valence state is in phase with the modulation of the integrated oxygen signal. We therefore conclude that the two newly formed interface layers observed in the BF-STEM images arise from oxide formation of the Cr [5]. The shift towards the O-K-edge indicates that the two formed chromium oxides at the two interfaces are not similar. We attribute this difference to the different origin of the chromium oxide. The thin interface is formed during Cr deposition onto the oxidized semiconductor allowing a chemical reaction and alloying between the Cr and the oxidized GaAs. The second, thicker oxide is formed when the chromium layer is exposed to air after metal deposition forming a pure chromium oxide.

As a last example for radial superlattices of a hybrid layer system, a HRTEM study of the rolled-up InGaAs/GaAs/1-hexadecanethiol trilayer [3] is carried out.

Figures 4(a) and 4(b) display HRTEM images of the produced radial semiconductor/organic superlattice after the roll-up of the thiolated InGaAs/GaAs layer system. The HRTEM images show the existence of crystalline areas as well as regions where no clear lattice image is present in the tube wall. It is known from the chemical analysis of such structures [3] that areas with a clear lattice image can be attributed to the InGaAs/GaAs bilayer. The areas with no clear lattice image are ascribed to the 1-hexadecanethiol layer due to its lack of translation symmetry. The measured layer thickness for the organic self-assembled monolayer is about 2 nm. This length is in good agreement with the length of the 1-hexadecanethiol molecule (2.1 nm, calculated using CS CHEM 3D PRO, version 7.0) and a chain tilt angle of 16° reported for methyl-terminated alkanethiolate monolayers on GaAs prepared from solution [18]. The measured 5.5 nm thickness of the rolled-up

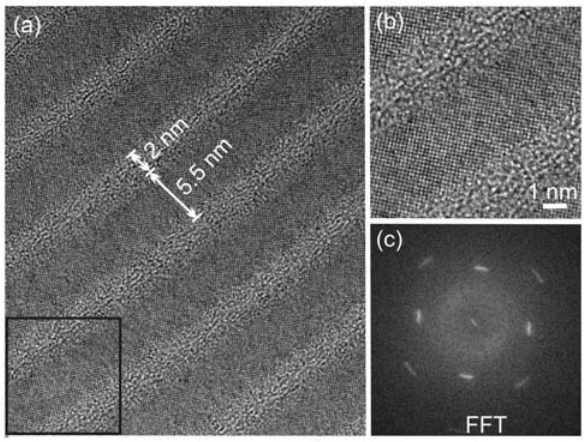

Figure 4 (a) HRTEM image of a radial InGaAs/GaAs/thiol superlattice. The single-crystalline semiconductor layers as well as the non-crystalline thiol layers can be identified. (b) Higher-magnification HRTEM image of a single period of the superlattice. In the image the lattice fringes of the InGaAs/GaAs single-crystalline bilayer can clearly be seen. (c) FFT of the HRTEM image of (a) verifying the good crystalline quality of the semiconductor layer with the fourfold symmetry of the zinc blende lattice.

InGaAs/GaAs bilayer agrees with the thickness of the bilayer in the unrolled area of the same sample. This result, together with a detailed chemical analysis (not shown here, see Ref. [3]), indicates that the thiol successfully protects the semiconductor layer against oxidation. The highly effective protection and passivation of GaAs surfaces by molecular self-assembled monolayers has been studied in detail previously [19]. Furthermore, in the case of a rolled-up radial superlattice, the hydrophobic nature of the thiolated GaAs possibly suppresses the incorporation of water from the wet chemical etching solution into the tube walls. Therefore, no additional interface region as observed in the two previously discussed hybrid layer systems is found.

Figure 4(c) displays the two-dimensional Fast Fourier Transformation (FFT) of the HRTEM image, revealing the fourfold symmetry typical for the zinc blende lattice along the <010>-zone axis. The FFT confirms that the zinc blende lattice of the epitaxial layer remains undamaged by the roll-up process and inherits its original crystal structure. Furthermore, a clear bending of the layers is visible in the overview HRTEM image of Fig. 4(a) as well as the slight elongation of the spots in the FFT indicating the formation of the radial symmetry during the roll-up of the layers [8].

4 Conclusions In conclusion, the fabrication of radial crystals and superlattices for various material systems has been demonstrated. Roll-up of strained pseudomorphic InGaAs/Fe_3Si layers demonstrate the realization of periodic structures out of an epitaxial system. The extension of the roll-up technique to layer systems such as InAlGaAs/GaAs/Cr and InGaAs/GaAs/thiol lifts the fundamental restriction of planar growth techniques, and combines single-crystalline and polycrystalline or non-crystalline layers into a unique periodic multilayer system. Detailed structural and chemical analysis of the obtained radial superlattices implies that interface formation plays a crucial role when discussing these new short-period superlattices.

The great impact of planar superlattices originates from their fascinating electronic, optical or magnetic properties. Thus, rolled-up hybrid radial superlattices seem attractive candidates to reveal fundamentally new electronic, optical or magnetic properties in future experiments.

Acknowledgements Experimental help and fruitful discussions with Y. F. Mei, E. Coric, B. Arnold, A. Güth, and D. J. Thumer are acknowledged. This work was financially supported by the BMBF (03N8711) and EC NoE Sandie.

References

[1] R. W. Kelsall, I. W. Hamley, and M. Geoghegan, Nanoscale Science and Technology (John Wiley & Sons, 2005).
[2] Ch. Deneke, N.-Y. Jin-Phillipp, I. Loa, and O. G. Schmidt, Appl. Phys. Lett. **84**, 4475 (2004).
[3] Ch. Deneke, U. Zschieschang, H. Klauk, and O. G. Schmidt, Appl. Phys. Lett. **89**, 263110 (2006).
[4] R. Songmuang, A. Rastelli, S. Mendach, and O. G. Schmidt, Appl. Phys. Lett. **90**, 091905 (2007)
[5] Ch. Deneke, W. Sigle, U. Eigenthaler, P. A. van Aken, G. Schütz, and O. G. Schmidt, Appl. Phys. Lett. **90**, 263107 (2007).
[6] V. Ya. Prinz, V. A. Seleznev, A. K. Gutakovsky, A. V. Chekhovskiy, V. V. Preobrazhenskii, M. A. Putyato, and T. A. Gavrilova, Physica E **6**, 828 (2000).
[7] O. G. Schmidt and K. Eberl, Nature **410**, 168 (2001).
[8] B. Krause, C. Mocuta, T. H. Metzger, Ch. Deneke, and O. G. Schmidt, Phys. Rev. Lett. **96**, 165502 (2006).
[9] Ch. Deneke and O. G. Schmidt, Appl. Phys. Lett. **89**, 123121 (2006).
[10] Ch. Deneke, U. Zschieschang, H. Klauk, and O. G. Schmidt, arxiv: condmat/0612373.
[11] J. Herfort, H. P. Schönherr, K. J. Friedland, and K. H. Ploog, J. Vac. Sci. Technol. B **22**, 2073 (2004)
[12] B. Jenichen, V. M. Kaganer, J. Herfort, D. K. Satapathy, H. P. Schönherr, W. Braun, and K. H. Ploog, Phys. Rev. B **72**, 075329 (2005)
[13] Y. F. Mei, D. J. Thurmer, F. Cavallo, S. Kiravittaya, O. G. Schmidt, Adv. Mater. **19**, 2124 (2007).
[14] Y. F. Mei, S. Kiravittaya, M. Benyoucef, D. J. Thurmer, T. Zander, Ch. Deneke, F. Cavallo, A. Rastelli, and O. G. Schmidt, Nano Lett. **7**, 1676 (2007).
[15] Ch. Deneke and O. G. Schmidt, Appl. Phys. Lett. **85**, 2914 (2004).
[16] N.-Y. Jin-Phillipp, J. Thomas, M. Kelsch, Ch. Deneke, R. Songmuang, and O. G. Schmidt, Appl. Phys. Lett. **88**, 033113 (2006).
[17] T. L. Daulton and B. J. Little, Ultramicroscopy **106**, 561 (2006).
[18] C. L. McGuiness, A. Shaporenko, C. K. Mars, S. Uppili, M. Zharnikov, and D. L. Allara, J. Am. Chem. Soc. **126**, 5231 (2006).
[19] S. R. Lunt, G. N. Fiyba, P. G. Santangelo, and N. S. Lewisa, J. Appl. Phys. **70**, 7449 (1991).

